Chemistry, Raman and infrared spectroscopic characterization of the phosphate mineral reddingite – $(MnFe)_3(PO_4)_2(H_2O,OH)_3$ a mineral found in lithium-bearing pegmatite

Ray L. Frost[a•], Yunfei Xi[a], Ricardo Scholz[b], Fernanda M. Belotti[c], Leonardo E. Lagoeiro[b]

[a*] *School of Chemistry, Physics and Mechanical Engineering, Science and Engineering Faculty, Queensland University of Technology, GPO Box 2434, Brisbane Queensland 4001, Australia.* r.frost@qut.edu.au

[b]*Geology Department, School of Mines, Federal University of Ouro Preto, Campus Morro do Cruzeiro, Ouro Preto, MG, 35,400-00, Brazil*

[c]*Federal University of Itajubá, Campus Itabira, Itabira, MG, 35,903-087, Brazil*

• Author to whom correspondence should be addressed (r.frost@qut.edu.au)
P +61 7 3138 2407 F: +61 7 3138 1804

Abstract

Detailed investigation of an intermediate member of the reddingite-phosphoferrite series, including infrared and Raman spectroscopy, scanning electron microcopy and electron microprobe analysis has been carried out on a homogeneous sample from a lithium bearing pegmatite named Cigana mine, near Conselheiro Pena, Minas Gerais, Brazil. The determined formula is $(Mn_{1.60}Fe_{1.21}Ca_{0.01}Mg_{0.01})_{\sum 2.83}(PO_4)_{2.12}\cdot(H_2O_{2.85}F_{0.01})_{\sum 2.86}$, indicating predominance in the reddingite member.

Raman spectroscopy coupled with infrared spectroscopy supports the concept of phosphate, hydrogen phosphate and dihydrogen phosphate units in the structure of reddingite-phosphoferrite. Infrared and Raman bands attributed to water and hydroxyl stretching modes are identified. Vibrational spectroscopy adds useful information to the molecular structure of reddingite-phosphoferrite.

Keywords: Raman, infrared, molecular structure, reddingite-phosphoferrite, phosphate, pegmatite

Introduction

Reddingite is a uncommon manganese hydrated phosphate mineral with general chemical formula expressed as $(MnFe)_3(PO_4)_2(H_2O,OH)_3$ and belongs to the phosphoferrite group. In general, members have the formula $(M1)(M2)_2(PO_4)_2(H_2O,OH)_3$. The mineral forms a complex triple series with phosphoferrite, its Fe^{2+} analogue and with kryzhanovskite, the Fe^{3+} analogue (Moore *et al.* 1980). Other minerals related to the group are landesite and garyansellite.

According to Tennyson (1954), reddingite crystallizes in orthorhombic symmetry of *Pmna* space group with unit-cell parameters a = 9.49 Å, b = 10.08 Å, c = 8.07 Å, V = 832.24 Å^3. It is a common mineral in lithium bearing pegmatites and is related to the hydrothermal alteration after triphylite-lithiophilite (Roda *et al.* 2004). Moore (1973) described phosphoferrite as a late hydrothermal mineral in the phosphate paragenesis of pegmatites. Nriagu and Dell (1974) carried out thermochemical studies for low temperature basic iron phosphates and suggest the formation of phosphoferrite-reddingite solid solution in phosphorus-rich sediments, during the diagenetic process, in reducing environments. The crystallization of authigenic minerals in sediments, develop an important function in the removal and storage of heavy metals and phosphate pollutants.

The crystal structures of phosphoferrite and kryzhanovskite were detemined by Moore and Araki (1976), and the similarities between the two crystal structures can be applied to the crystal structure of reddingite. The structure is based on sheets of corner- and edge-linked octahedra which are oriented parallel to {100}.

58 The phosphate tetrahedra are situated between these symmetry-equivalent
59 octahedral sheets and link by corner sharing. As a result, the structure is a rather
60 rigid framework of octahedra and tetrahedra and the crystals exhibit no good
61 cleavage.
62
63 As suggested by Moore and Araki (1976), the mechanism of oxidation of Fe^{2+} to
64 Fe^{3+} in the phosphoferrite-kryzhanovskite series can be expressed as $2Fe^{2+}(H_2O)$
65 $\rightarrow 2Fe^{3+}(OH)^- + H_2$. The presence of OH^- anion is indicative of Fe^{3+} in the
66 structure. Studies concerning the mineralogy of phosphoferrite group minerals are
67 rare in the literature (Sturman and Dunn 1978; Dill *et al.* 2009) and data about
68 spectroscopic characterization are restricted to the database of the University of
69 Arizona (rruff.info); however no interpretation is given. In the study of similar
70 phases, infrared spectroscopic characterization of manganese phosphate
71 pentahydrate calcined at 400°C was carried out by Sarawadekar and Kulkarni
72 (1983), who also described the dehydration at temperatures up to 405°C. No
73 Raman spectroscopic investigation of these phosphate phases related to the
74 phosphoferrite group has been published. However, in recent years, the
75 application of spectroscopy to understand the structure of phosphates has been on
76 the increase (Dias *et al.* 2011; Frost and Xi 2012).
77
78 S. D. Ross in Farmer's treatise (1974) divided the vibrational spectra of
79 phosphates according to the presence, or absence of water and/or hydroxyl units.
80 In aqueous systems, the Raman spectra of phosphate oxyanions show a symmetric
81 stretching mode (ν_1) at 938 cm^{-1}, the antisymmetric stretching mode (ν_3) at 1017
82 cm^{-1}, the symmetric bending mode (ν_2) at 420 cm^{-1} and the ν_4 out-of-plane
83 bending mode at 567 cm^{-1}. The value for the ν_1 symmetric stretching vibration of

PO_4 units as determined by infrared spectroscopy was also described (Frost *et al.* 2002a; 2002b; 2002c). The position of the symmetric stretching vibration is mineral dependent and a function of the cation and crystal structure. The fact that the symmetric stretching mode is observed in the infrared spectrum affirms a reduction in symmetry of the PO_4 units.

The value for the ν_2 symmetric bending vibration of PO_4 units as determined by infrared spectroscopy was given as 438 cm^{-1} (augelite), 452 cm^{-1} (wavellite), 440 and 415 cm^{-1} (rockbridgeite), 455, 435 and 415 cm^{-1} (dufrenite) and 470 and 450 cm^{-1} (beraunite). The observation of multiple bending modes provides an indication of symmetry reduction of the PO_4 units. This symmetry reduction is also observed through the ν_3 antisymmetric stretching vibrations. Augelite shows infrared bands at 1205, 1155, 1079 and 1015 cm^{-1} (Frost and Weier 2004); wavellite at 1145, 1102, 1062 and 1025 cm^{-1}; rockbridgeite at 1145, 1060 and 1030 cm^{-1}; dufrenite at 1135, 1070 and 1032 cm^{-1}; and beraunite at 1150, 1100, 1076 and 1035 cm^{-1}.

In the infrared study of triploidite, a basic manganese phosphate, Farmer reports the infrared spectrum with the (ν_1) at 957 cm^{-1}, (ν_3) at 1090, 1058, 1030 and 1010 cm^{-1}, (ν_2) at 420 cm^{-1} and the ν_4 mode at 595, 570, 486 cm^{-1} (Frost and Xi 2012). A hydroxyl stretching wavenumber of 3509 cm^{-1} was tabled. In the infrared spectroscopic study of strengite, in the region below 400 cm^{-1}, Frost and Weier (2004) described the metal stretching vibrations for MnO and the OMnO bending modes.

In this work, samples of a pure, monomineral reddingite from the Cigana pegmatite, located in the municipality of Conselheiro Pena, Brazil has been carried out. Studies include chemistry with analysis via electron microprobe (EMP) in the WDS mode and the spectroscopic characterization of the structure with infrared and Raman.

Experimental

Samples description and preparation

The reddingite samples were collected from the Cigana mine (also named Jocão Claim), a lithium-bearing pegmatite located in the Conselheiro Pena Pegmatite district (CPD), one of the eleven metallogenetic subdivisions of the Eastern Brazilian Pegmatite Province (EBP)(in Minas Gerais (Pedrosa Soares *et al.* 2011). Geological description of the CPD and the complete paragenesis of the Cigana pegmatite has been described by Chaves *et al*., (2005).

In the Cigana mine, brown reddish reddingite crystals up to 4.0 mm along the **c** axis with octahedral morphology occur in association with vivianite, lithiophilite and hureaulite. The sample came from the collection of the Geology Department of the Federal University of Ouro Preto, Minas Gerais, Brazil, with sample code SAA-081. The reddingite crystals were hand selected. The sample was gently crushed and the associated minerals were removed under a stereomicroscope Leica MZ4. The reddingite crystals were phase analyzed by X-ray diffraction. Scanning electron microscopy (SEM) was applied to support the chemical characterization and indicate the elements to be analysed by EMP. Thermogravimetric analysis was undertaken to support the H_2O determination.

X-ray diffraction (XRD)

Powder X-ray diffractograms (XRD) were obtained with a PANalytical Empyrean diffractrometer equipped with a Cu-tube and a nickel filter in the facilities of the Geology Department of the Federal University of Ouro Preto. The scanning was done at 25°C from 4° to 70° (2θ) at 0.25° per minute with an X-ray accelerator, using silicon as external standard. Cell parameters were calculated by Rietveld refinement using intensity and angular weighting of the most intense peaks.

Thermogravimetric analysis - TG/DTG

Thermogravimetric analysis of the reddingite mineral were obtained by using TA Instruments Inc. Q500 high- resolution TGA operating at a 5 °C/min ramp with 6.0 °C resolution from room temperature to 1000 °C in a high-purity flowing nitrogen atmosphere (40 cm^3/min). Approximately 65 mg of finely ground dried sample was heated in an open platinum crucible.

Electron microprobe analysis (EMP)

EMP was performed in a reddingite single crystal. The chemical analysis was done on a Jeol JXA8900R with four WDS spectrometers at the Physics Department of the Federal University of Minas Gerais, Belo Horizonte. For each selected element the following standards were applied: Mn (rhodonite), Fe (magnetite), Ca ($Ca_2P_2O_7$), Mg (MgO), F (Fluorite) and P ($Ca_2P_2O_7$). Samples of reddingite embedded in an epoxy resin were coated with a thin layer of evaporated carbon. The EMPA was performed at 15 kV of accelerating voltage and beam current of 10 nA.

Raman microprobe spectroscopy

Crystals of reddingite were placed on a polished metal surface on the stage of an Olympus BHSM microscope, which is equipped with 10x, 20x, and 50x objectives. The microscope is part of a Renishaw 1000 Raman microscope system, which also includes a monochromator, a filter system and a CCD detector (1024 pixels). The Raman spectra were obtained using a Spectra-Physics model 127 He-Ne laser producing highly polarised light at 633 nm and collected at a nominal resolution of 2 cm^{-1} and a precision of ± 1 cm^{-1} in the range between 200 and 4000 cm^{-1}. Repeated acquisitions on the crystals using the highest magnification (50x) were accumulated to improve the signal to noise ratio of the Raman spectra. Raman Spectra were calibrated using the 520.5 cm^{-1} line of a

silicon wafer. The Raman spectrum of at least 10 crystals was collected to ensure the consistency of the spectra.

Infrared spectroscopy

Infrared spectra were obtained using a Nicolet Nexus 870 FTIR spectrometer with a smart endurance single bounce diamond ATR cell. Spectra over the 4000–525 cm^{-1} range were obtained by the co-addition of 128 scans with a resolution of 4 cm^{-1} and a mirror velocity of 0.6329 cm/s. Spectra were co-added to improve the signal to noise ratio. The infrared spectra are given in the supplementary information.

Spectral manipulation such as baseline correction/adjustment and smoothing were performed using the Spectracalc software package GRAMS (Galactic Industries Corporation, NH, USA). Band component analysis was undertaken using the Jandel 'Peakfit' software package that enabled the type of fitting function to be selected and allows specific parameters to be fixed or varied accordingly. Band fitting was done using a Lorentzian-Gaussian cross-product function with the minimum number of component bands used for the fitting process. The Gaussian-Lorentzian ratio was maintained at values greater than 0.7 and fitting was undertaken until reproducible results were obtained with squared correlations of r^2 greater than 0.995.

Results and discussion

Mineralogical and chemical characterization

The mineral phase reddingite was identified by XRD and the difractogram is shown in the Figure 1. The unit cell paramethers were calculated by Rietveld refinement and are given as: a = 9.4889 (7), b = 10.1260 (7) and c = 8.7102 (6) Å. The calculated values are in agreement with the phosphoferrite group and the published data for reddingite (Tennyson, 1954).

The quantitative chemical analysis of reddingite is presented in Table 1. Composition is the result of in the average of four spots. H_2O content was measured by mass loss (ML) observed in the TG curve (Figure 2), where ML = H_2O + F. The chemical formula was calculated on the basis of 11 oxygen atoms (O, H_2O, F) in the structure. The spectroscopic characterization carried out in this work indicates the presence of H_2O in the structure and the absence of OH^-.The TG curve of reddingite shows a total mass loss of 12.91% on heating to 950ºC in nitrogen flux.

The chemical composition indicates an intermediate member of the reddingite-phosphoferrite series with predominance of reddingite in relation to the phosphoferrite end member. The chemical analysis shows 28.44% of MnO and 21.87% of FeO. Traces of Ca and Mg were also found (0.10% CaO and 0.06% MgO). Due to the absence of OH^- in the structure as supported by infrared and Raman spectroscopy, the total iron content is considered as Fe^{2+}, as shown in the chemical formula:

$$(Mn_{1.60}Fe_{1.21}Ca_{0.01}Mg_{0.01})_{\sum 2.83}(PO_4)_{2.12}\cdot(H_2O_{2.85}F_{0.01})_{\sum 2.86}$$

221 **Spectroscopy**

222 The Raman spectrum over the 100 to 4000 cm^{-1} spectral range is displayed in
223 Figure 3a. This figure shows the relative intensity and position of the various
224 bands. There are parts of the spectrum where no intensity is observed. Therefore,
225 the spectrum is subdivided into sections depending upon the types of vibration
226 being studied. The infrared spectrum of reddingite is reported in Figure 3b. In a
227 similar fashion, the IR spectrum is divided into sections for further detailed
228 analysis. The Raman spectrum of reddingite in the 800 to 1400 cm^{-1} spectral
229 range is shown in Figure 4a. The spectrum is dominated by a sharp band at 970
230 cm^{-1} which may be deconvoluted into component bands at 951, 963 and 970 cm^{-1}.
231 This band is attributed to the symmetric PO_4^{3-} stretching vibration. A second
232 strong Raman band at 1007 cm^{-1} is attributed to symmetric $HOPO_3^{2-}$ stretching
233 vibration. The series of low intensity Raman bands at 1064, 1093, 1104 and 1193
234 cm^{-1} are assigned to the PO_4^{3-} and $HOPO_3^{2-}$ antisymmetric stretching vibrations.
235 In the infrared spectrum (Figure 4b), a broad spectral profile is observed with
236 curve resolved band components delineated at 959, 1004, 1026, 1054 and 1086
237 cm^{-1}. These bands are a combination of the PO_4^{3-} and $HOPO_3^{2-}$ antisymmetric and
238 symmetric stretching vibrations. The low intensity infrared bands centered upon
239 673 and 739 cm^{-1} are thought to be due to water librational modes. The
240 observation of multiple bands supports the concept that not all the water
241 molecules in the structure of reddingite are equivalent.

242

243 The Raman spectrum of reddingite in the 300 to 800 cm^{-1} spectral range and in the
244 100 to 300 cm^{-1} spectral range are reported in Figures 5a and 5b. An intense
245 Raman band at 588 cm^{-1} with shoulders at 549 and 569 cm^{-1} are assigned to the ν_4
246 out of plane bending modes of the PO_4 and $HOPO_3$ units. The series of bands at

420, 458, 482, 504 and 531 cm^{-1} are attributed to the ν_2 PO_4 and $HOPO_3$ bending modes. The low intensity Raman bands at 330 and 373 cm^{-1} are attributed to metal-oxygen stretching vibrations. In the far low wavenumber region, strong Raman bands are found at 144, 164 and 179 cm^{-1} with bands of lower intensity at 223, 241, 260 and 286 cm^{-1}. These bands are due to external vibrations and may simply be described as lattice vibrations.

The Raman spectrum of reddingite in the OH stretching region is illustrated in Figure 6a, whilst the infrared spectrum in the 2800 to 3800 cm^{-1} spectral range is reported in Figure 6b. The Raman spectrum of reddingite displays a very intense band at 3445 cm^{-1} with a shoulder at 3265 cm^{-1} and is assigned to water stretching vibrations. In contrast, the infrared spectrum shows a series of overlapping bands in quite a broad spectral profile. Infrared bands are observed at 3061, 3225, 3399 and 3459 cm^{-1}. These bands are assigned to a combination of water antisymmetric and symmetric stretching modes. The position of the bands in both the Raman and infrared spectra supports the concept that the water molecules are involved in quite strong hydrogen bonding in the structure of reddingite. This concept is supported by the observation of water bending modes observed at 1641 cm^{-1} in the Raman spectrum and 1637 cm^{-1} in the infrared spectrum (Figure 7a and 7b). These bands are due to the bending modes of quite strongly hydrogen bonded water. In non-hydrogen bonded water as may be found in water vapour the band occurs at 1595 cm^{-1}. In weakly hydrogen bonded systems, the band occurs at 1620 cm^{-1}.

Conclusions

An intermediate member of the reddingite-phosphofillite series was studied by Raman and infrared spectroscopy. The chemical characterization was carried out by EMP and shows chemical formula expressed by $(Mn_{1.60},Fe_{1.21},Ca_{0.01},Mg_{0.01})_{\sum 2.83}(PO_4)_{2.12}(H_2O_{2.85},F_{0.01})_{\sum 2.86}$, that indicate predominance in the reddingite member.

The spectroscopic study indicates the presence of H_2O and the absence of OH^- in the structure. Raman assigned band to water stretching vibrations were observed in the region of 3445 cm^{-1} and 3265 cm^{-1}. The infrared spectrum shows a series of overlapping bands at 3061, 3225, 3399 and 3459 cm^{-1}, assigned to a combination of water antisymmetric and symmetric stretching modes. The absence of OH^- suggests the presence of Fe^{2+}. Vibrational spectroscopy enables new knowledge on the structure of reddingite to be understood.

Acknowledgements

The financial and infra-structure support of the Discipline of Nanotechnology and Molecular Science, Science and Engineering Faculty of the Queensland University of Technology, is gratefully acknowledged. The Australian Research Council (ARC) is thanked for funding the instrumentation. We also gratefully acknowledge the contributions of the Fundação de Amparo à Pesquisa do Estado de Minas Gerais – FAPEMIG - grant No. CRA - APQ-03998-10.

294 **References**

295

296 Chaves MLSC, Scholz R, Atencio D, Karfunkel J (2005) Assembléias e
297 paragêneses minerais singulares nos pegmatitos da região de Galiléia (Minas
298 Gerais) Geociências, 24:14 –161 (in Portuguese)

299

300 Dias LN, Pinheiro MVB, Moreira RL, Krambrock K, Guedes K, Menezes Filho
301 LAD, Karfunkel J, Schnellrath J, Scholz R (2011) Spectroscopic characterization
302 of transition metal impurities in natural montebrasite/amblygonite. Amer Min
303 96:42-52.

304

305 Dill HG, Weber B, Gerdes A, Melcher F (2009) The Fe-Mn phosphate aplite
306 'Silbergrube' near Waidhaus, Germany: epithermal phosphate mineralization in
307 the Hagendorf-Pleystein pegmatite province. Min Mag 7:1119 – 1144.

308

309 Farmer VC (1974) Mineralogical Society Monograph 4: The Infrared Spectra of
310 Minerals, The Mineralogical Society, London, pp. 427.

311

312 Frost RL, Martens W, Williams PA, Kloprogge JT (2002a) Raman and infrared
313 spectroscopic study of the vivianite-group phosphates vivianite, baricite, and
314 bobierrite. Min Mag 66:1063-1073.

315

316 Frost RL, Martens WN, Kloprogge T, Williams PA (2002b) Vibrational
317 spectroscopy of the basic manganese, ferric and ferrous phosphate minerals:
318 strunzite, ferristrunzite and ferrostrunzite. Neues Jb Miner Monat 11:481-496.

319

320 Frost RL, Williams PA, Martens W, Kloprogge JT, Leverett P (2002c) Raman
321 spectroscopy of the basic copper phosphate minerals cornetite, libethenite,
322 pseudomalachite, reichenbachite and ludjibaite. J. Raman Spectrosc 33:260-263.
323

324 Frost RL, Xi Y (2012) Molecular structure of the phosphate mineral brazilianite
325 $NaAl_3(PO_4)_2(OH)_4$: a semi precious jewel. J Mol Struc 1010:179-183.
326

327 Frost, RL Weier ML (2004) Vibrational spectroscopy of natural augelite. J Mol
328 Struc 697:207-211.
329

330 Moore PB (1973) Pegmatite phosphates: descriptive mineralogy and crystal
331 chemistry. Min Rec 4:103-130.
332

333 Moore PB, Araki T (1976) A mixed-valence solid-solution series: crystal structure
334 of phosphoferrite $(Fe^{2+})_3(H_2O)_3[PO_4]_2$. Inorg Chem 15:316-321.
335

336 Moore PB, Araki T, Kampf AR (1980) Nomenclature of the phosphoferrite
337 structure type: refinements of landsite and kryzhanovskite. Min Mag 43:789-795.
338

339 Nalini HA (1997) Caractérisation dês suítes magmatiques néoprotérozóiques de la
340 region de Conselheiro Pena et Galiléia (Minas Gerais, Brésil). These de Docteur,
341 Graduate School of Engineering, Ecole Nationale Superieure dês Mines de Saint
342 Etienne, 237 pp. (in French).
343

Nriagu, JO, Dell CI (1974) Diagenetic formation of iron phosphates in recent lake sediments. Arner Min 59, 934-946.

Pedrosa-Soares AC, Campos CM de, Noce CM, Silva LC da, Novo TA, Roncato J, Medeiros SM, Castañeda C, Queiroga GN, Dantas E, Dussin IA, Alkmim F (2011) Late Neoproterozoic-Cambrian granitic magmatism in Araçuaí orogen (Brazil), the Eastern Brazilian Pegmatite Province and related mineral resources. Geological Society Special Publication, 350: 25-51.

Roda E, Pesquera A, Fontan F, Keller P (2004) Phosphate mineral associations in the Cañada pegmatite (Salamanca, Spain) : Paragenetic relationships, chemical compositions, and implications for pegmatite evolution. Amer Min 89:110-125.

Sarawadekar RG, Kulkarni SB (1983) Physico-chemical properties of metal phosphates. Thermochim Acta 67:341-349.

Sturman BD, Dunn PJ (1984) Garyansellite, a new mineral from Yukon Territory, Canada. Amer Min 69:207-209.

Tennyson C (1954) Phosphoferrit und reddingit von Hagendorf, Neues Jb Miner Monat Ab 87:185-217.

370
371 **List of Tables**

372

373 **Table 1. Chemical composition of reddingite-phosphoferrite from Cigana**
374 **pegmatite (mean of 4 electron microprobe analyses). H_2O calculated by**
375 **thermogravimetric analysis.**

Constituent	wt.%	Number of Cations	Range (wt.%)	Probe Standard
MnO	28.44	1.60	27.10 – 29.82	Rhodonite
FeO	21.87	1.21	19.44 – 24.44	Magnetite
CaO	0.10	0.01	0.02 – 0.22	$Ca_2P_2O_7$
MgO	0.06	0.01	0.02 – 0.18	MgO
P_2O_5	37.70	2.12	36.17 – 38.39	$Ca_2P_2O_7$
H_2O	12.91	2.85	Calculated by loss of mass (TG)	
F	0.06	0.01	0.00 – 0.19	Fluorite
O-F	-0.03			
Total	101.17			

376

377

378

379

380

381

382

383 **List of Figures**

384 Figure 1 X-ray diffraction pattern of reddingite at 25°C. The two most intense
385 peaks are shown.

386

387 Figure 2 – TG/DTG pattern of reddingite

388

389 Figure 3 (a) Raman spectrum of reddingite in the 100 to 4000 cm^{-1} spectral range
390 (b) Infrared spectrum of reddingite in the 500 to 4000 cm^{-1} spectral range.

391

392 Figure 4 (a) Raman spectrum of reddingite in the 800 to 1400 cm^{-1} spectral range
393 (b) Infrared spectrum of reddingite in the 500 to 1300 cm^{-1} spectral range.

394

395 Figure 5 (a) Raman spectrum of reddingite in the 300 to 800 cm^{-1} spectral range
396 (b) Raman spectrum of reddingite in the 100 to 300 cm^{-1} spectral range

397

398 Figure 6 (a) Raman spectrum of reddingite in the 2800 to 3800 cm^{-1} spectral range
399 (b) Infrared spectrum of reddingite in the 2800 to 3800 cm^{-1} spectral range.

400

401 Figure 7 (a) Raman spectrum of reddingite in the 1400 to 1800 cm^{-1} spectral range
402 (b) Infrared spectrum of reddingite in the 1300 to 1800 cm^{-1} spectral range.
403

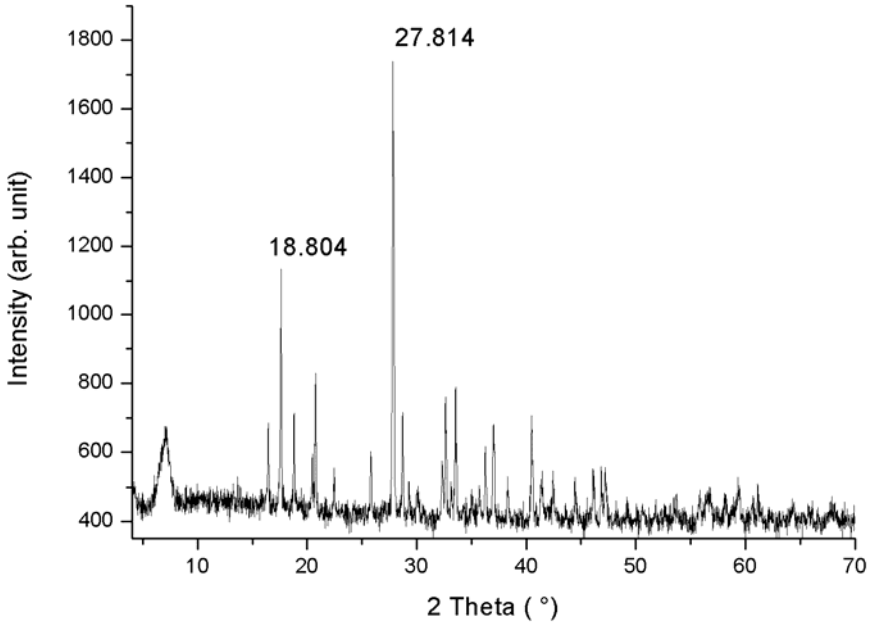
27.814
18.804
Intensity (arb. unit)
2 Theta (°)
1800
1600
1400
1200
1000
800
600
400
10
20
30
40
50
60
70

Figure 1

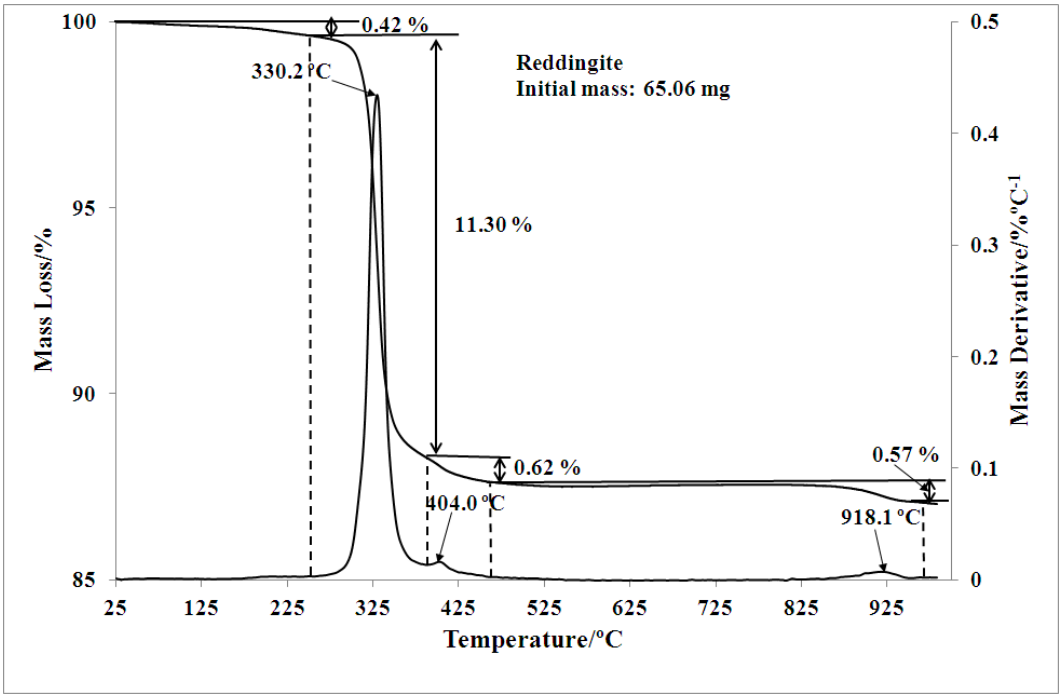

420

421 **Figure 2**

422

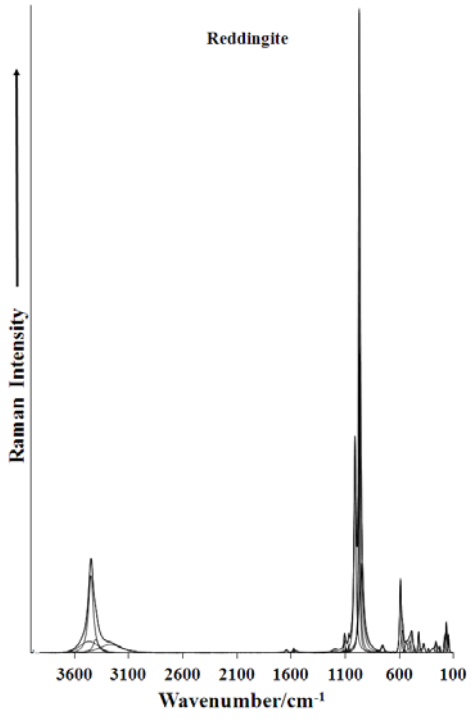

Figure 3a

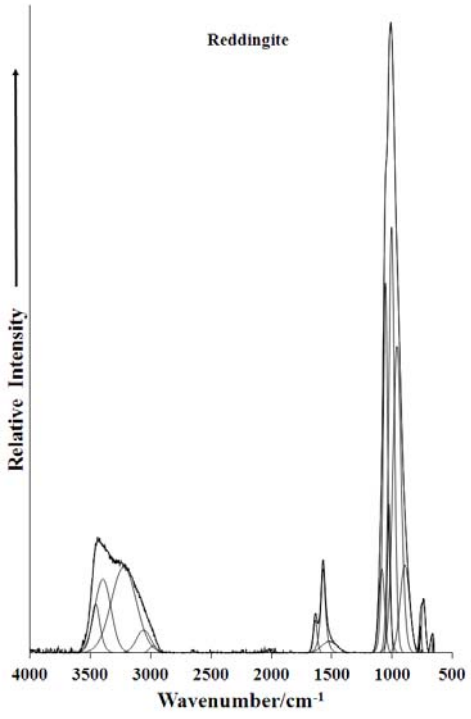

Figure 3b

423

424

425

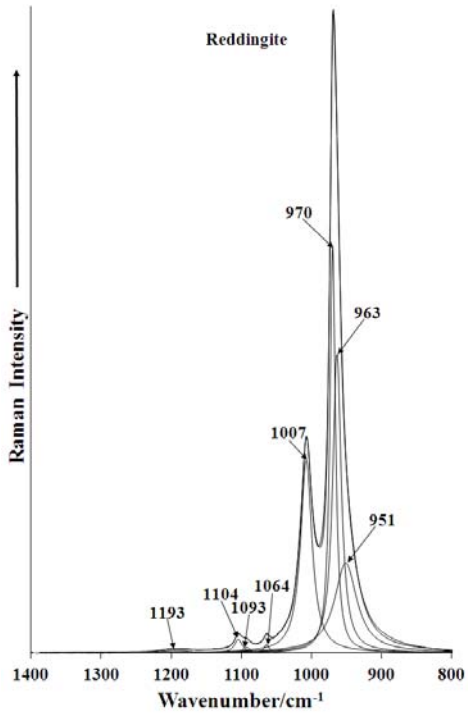

Figure 4a

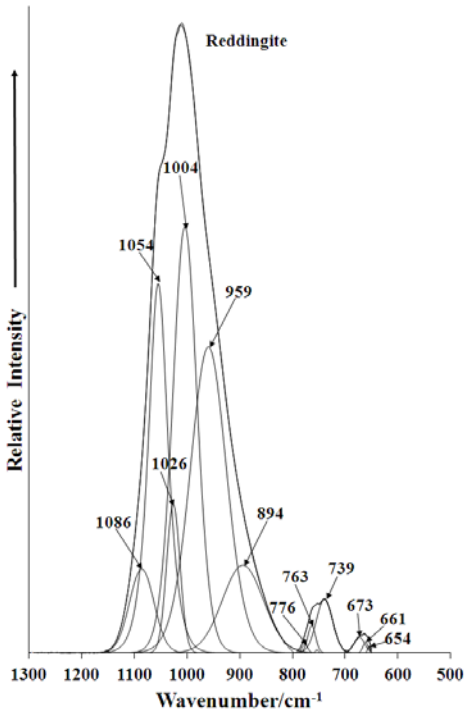

Figure 4b

426

427

428

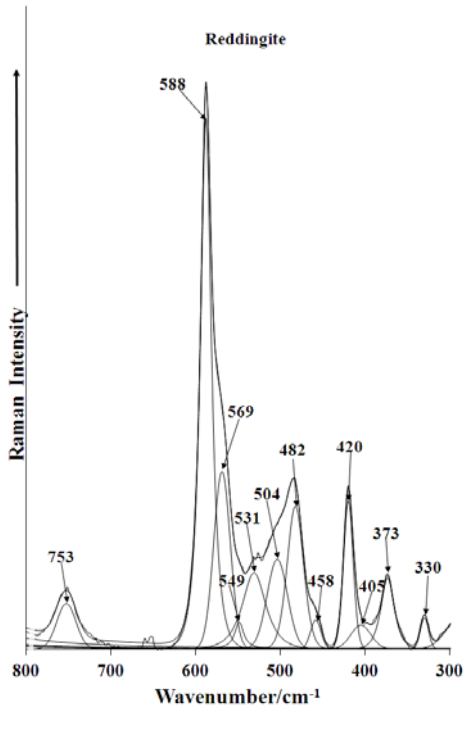

Figure 5a

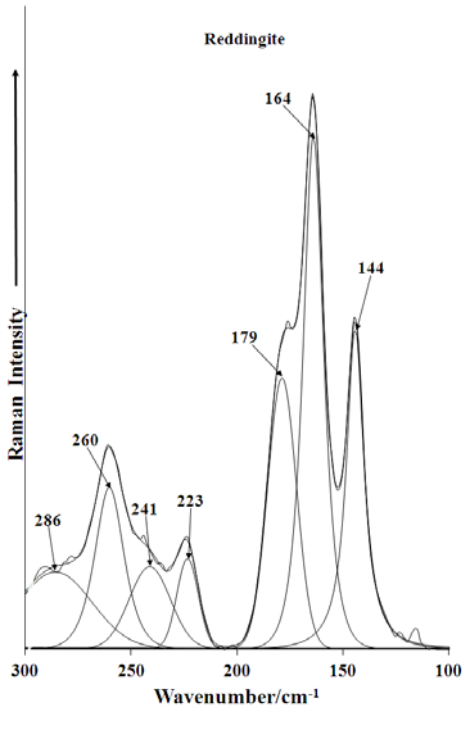

Figure 5b

429

430

431

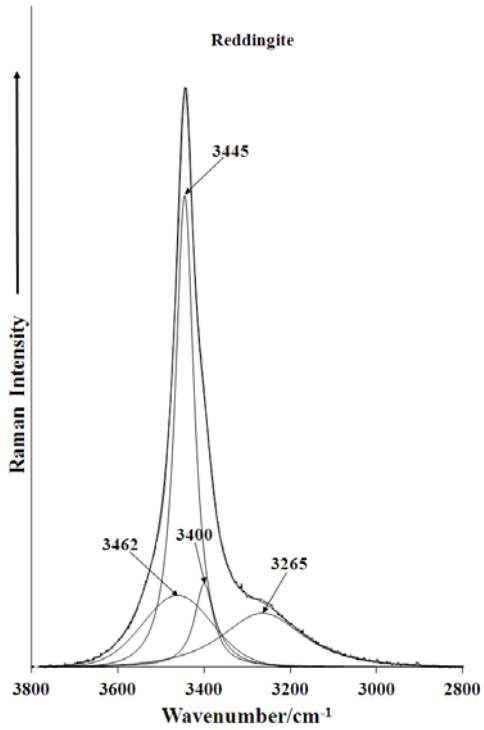

Figure 6a

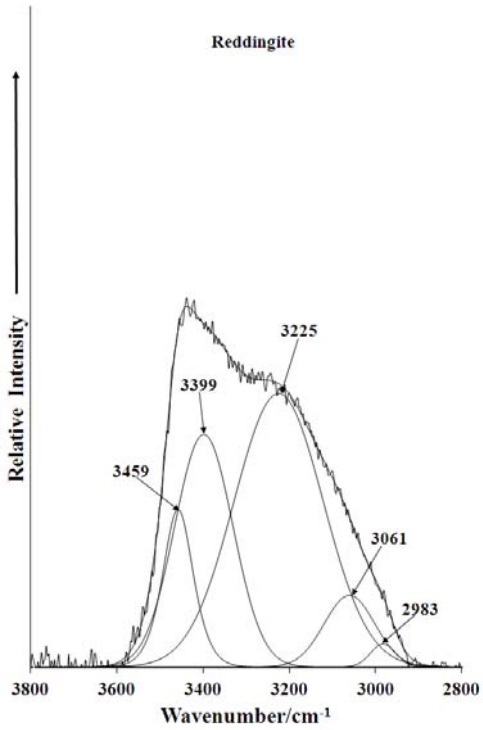

Figure 6b

432

433

434

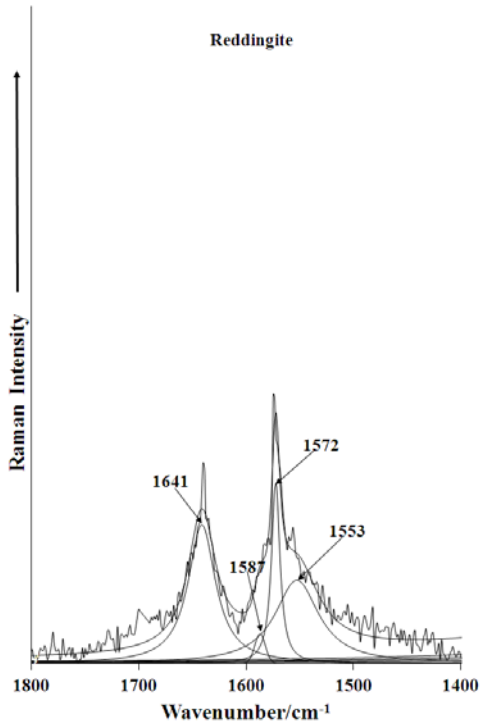

Figure 7a

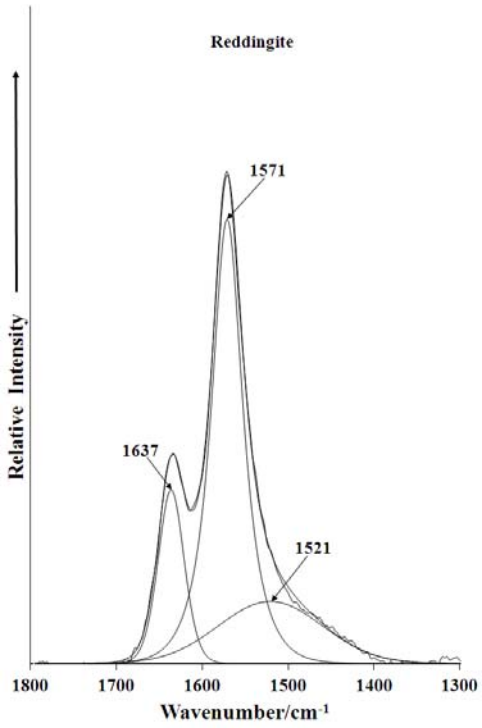

Figure 7b

435

436

437

438

439